JOURNAL OF GUIDANCE, CONTROL, AND DYNAMICS
Vol. 43, No. 1, January 2020

Engineering Notes

Linear Coupled Attitude–Orbit Control Through Aerodynamic Drag

Andrew T. Harris*
University of Colorado Boulder, Boulder, Colorado 80309
Christopher D. Petersen†
U.S. Air Force Research Laboratory, Kirtland Air Force Base, New Mexico 87123
and
Hanspeter Schaub‡
University of Colorado Boulder, Boulder, Colorado 80309-0431

https://doi.org/10.2514/1.G004521

I. Introduction

ATMOSPHERIC forces on spacecraft have long been recognized as an avenue for coupling between attitude and orbital dynamics [1]. Owing to its dependence on atmospheric density, these forces and torques are small relative to gravity and are typically considered as perturbations in the context of orbital motion. However, at low-Earth-orbit (LEO) altitudes, forces from atmospheric interactions can have substantial impacts on spacecraft orbits [2]. For spacecraft that lack the volume or mass to mount thrusters (such as CubeSats) or those for which the thrusters are disabled but maintain attitude control through other means, the coupling between the attitude and orbital motion through drag presents one method of recovering mission utility. Additionally, there is rising interest in large LEO constellations for telecommunication and Earth imaging. In this context, drag-enabled attitude–orbit coupling could provide a propellant-free method for formation constitution and maintenance, thereby extending mission lifetimes and reducing constellation costs. This work aims to extend attitude-driven formation flight techniques to convex spacecraft geometries in a linear sense by exploiting attitude–orbit coupling under atmospheric drag.

In concept, the work presented here is similar to an existing body of literature that focuses on ballistic-coefficient controlled differential-drag formation flight. These techniques focus on the control of one or more spacecraft's ballistic coefficients by means of actuated flaps [3] or panels, and they treat either the ballistic coefficient or the spacecraft flow-wise projected area as the primary control input [4]. This class of differential-drag-based control was flown by the AeroCube-4 technology demonstration mission [5]. The addition of actuated flaps and panels, although attractive for control purposes, unfortunately adds additional costs and system complexity that are undesirable for mission managers. Many spacecraft, including CubeSats, have nonuniform geometries for which the projected areas vary with attitude, as demonstrated in Fig. 1; by adjusting the spacecraft's orientation with respect to the flow, accelerations from drag can be modulated, and therefore potentially used for control.

Horsley et al. [6] presented one method for incorporating the limitations of purely geometric-driven differential-drag control as part of a two-step nonlinear planning and control routine. Discrete-attitude configurations are selected to produce positive, negative, and zero relative accelerations, effectively using the spacecraft attitude to provide "bang–bang" orbit control. A similar approach based on discrete high- and low-drag attitude modes is used operationally by Planet Labs for constellation constitution and maintenance on their large-scale Earth-imaging CubeSat constellation [7]. This approach does not require complex, online modeling of spacecraft geometries and provides the maximum possible differential drag for a pair of spacecraft. However, the bang–bang approach used by many discrete-attitude-mode controllers incurs substantial mission costs, due to both the time needed to conduct a maneuver and the potentially large-attitude maneuvers needed to modulate the spacecraft attitude between configurations.

For CubeSats (such as Planet Lab's Dove spacecraft, shown in Fig. 1), maneuvering between a minimum-drag and maximum-drag configuration requires a 90 deg slew. As such, spacecraft are not capable of conducting mission operations during orbit maintenance periods. Dell'Elce and Kerschen [8] presented a method of single-axis attitude-driven orbit control for the QB50 constellation using an online optimizer and compensator. The computational intensiveness of this technique requires the use of approximations for online application but, nevertheless, provides credibility to the concept of continuous differential-drag control using small-attitude motions. Prior work [9] focused on the linearized dynamics of single-facet spacecraft; this work aims to extend this methodology to general spacecraft that can be modeled as collections of facets, allowing for the incorporation of higher-fidelity geometric models.

This work aims to improve upon computationally expensive optimization-based approaches by demonstrating a linear control approach for attitude-driven differential-drag formation flight. To do so, the coupling between spacecraft geometries and experienced drag through attitude must be explored directly. The influence of geometry and surface material properties on spacecraft drag is a subject of intense research due to its importance in both space object tracking and aeronomy studies. For analytic insight, facet-based models such as those explored by Sutton [10] provide reasonable accuracy and insight into the dynamics of the "true" system. An alternative approach is the use of multiparticle Monte Carlo (MC) or other MC-based methods to develop lookup tables or fitted analytical functions to approximate the real drag behavior of a given spacecraft. Although potentially more accurate in the presence of concave geometries [11], simple convex geometries (such as those of CubeSats) are reasonably well modeled by analytical expressions. In contrast to previous work, this Note explicitly considers models of multifaceted spacecraft and examines the effect of additional substantial perturbation dynamics on the control's performance.

Coupling between translational and rotational motions has been treated extensively in the context of robotics, providing a beneficial framework for analyzing problems in astrodynamics. Filipe and Tsiotras [12] developed a methodology for conducing coupled rotational–translational control for spacecraft rendezvous using a dual-quaternion representation of the attitude and orbit. Solar or electric sails, which also experience considerable attitude–orbit coupling, have served as the objects of study for coupled attitude–orbit control [13,14]. A common issue with these approaches is the

Presented as Paper 2018-0962 at the 2018 Space Flight Mechanics Meeting, Kissimmee, FL, 8–12 January 2018; received 17 April 2019; revision received 1 August 2019; accepted for publication 2 August 2019; published online 31 October 2019.

*Research Assistant, Ann and H.J. Smead Department of Aerospace Engineering Sciences, Graduate Student. Member AIAA.
†Research Engineer, Space Vehicles Directorate. Member AIAA.
‡Alfred T. and Betty E. Look Professor of Engineering, Department of Aerospace Engineering Sciences, Colorado Center for Astrodynamics Research, 431 UCB. Fellow AIAA.

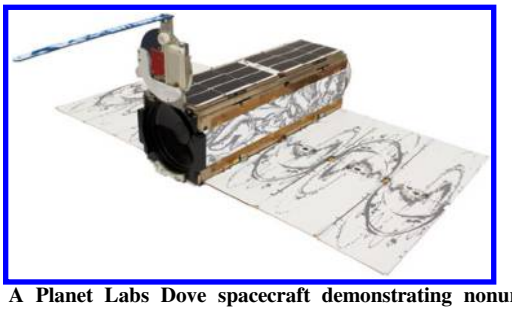

Fig. 1 A Planet Labs Dove spacecraft demonstrating nonuniform geometry.

lack of additional intuition gained through the use of compact translation–rotation representations such as dual quaternions. For these reasons, a straightforward linear model of the underling relative dynamics is sought.

The work is organized as follows. First, a nonlinear model of coupled attitude–orbit motion is presented in Sec. II.B. Next, this model is linearized about a selected reference orbit experiencing drag forces in Sec. II.D. Section II.E describes the novel linearization of the system's geometric attitude dependence about a selected reference attitude. The linear controllability of this system is established in Sec. III.A, which additionally describes necessary conditions for controllability. Finally, Sec. III.B.1 demonstrates the implementation and performance of a linear-quadratic regulator based on the linearized system on both the linearized and nonlinear dynamics under realistic variations from the assumed linear system.

II. Problem Statement

A. Frame Definitions

Before addressing the system model, it is important to define the reference frames that define the problem. The first is the planet-centered inertial frame N, which is taken as the global origin of the system:

$$N = \{\boldsymbol{0}, \hat{\boldsymbol{n}}_1, \hat{\boldsymbol{n}}_2, \hat{\boldsymbol{n}}_3\} \tag{1}$$

The next one is the Hill frame H, which is centered on the spacecraft at a given position $\boldsymbol{r}_{H/N}$ in orbit and consists of the following unit vectors:

$$H = \left\{\boldsymbol{r}_{H/N}, \hat{\boldsymbol{h}}_r, \hat{\boldsymbol{h}}_\theta, \hat{\boldsymbol{h}}_h\right\} \tag{2}$$

where $\boldsymbol{r}_{H/N}$ is the position vector of the spacecraft with respect to the center of the N frame, and the unit vectors are defined as follows:

$$\hat{\boldsymbol{h}}_r = \frac{\boldsymbol{r}_{H/N}}{\|\boldsymbol{r}_{H/N}\|} \tag{3}$$

$$\hat{\boldsymbol{h}}_h = \frac{\boldsymbol{r}_{H/N} \times \dot{\boldsymbol{r}}_{H/N}}{\|\boldsymbol{r}_{H/N} \times \dot{\boldsymbol{r}}_{H/N}\|} \tag{4}$$

$$\hat{\boldsymbol{h}}_\theta = \hat{\boldsymbol{h}}_h \times \hat{\boldsymbol{h}}_r \tag{5}$$

The direction cosines matrix that maps vectors from H to N, denoted as $[HN]$, is expressed by

$$[HN] = \begin{bmatrix} \hat{\boldsymbol{h}}_r^T \\ \hat{\boldsymbol{h}}_\theta^T \\ \hat{\boldsymbol{h}}_h^T \end{bmatrix} \tag{6}$$

The angular velocity of H with respect to N is given by the spacecraft's mean motion n, which forms the angular velocity vector ${}^{\mathcal{N}}\boldsymbol{\omega}_{H/N} = \dot{f}\hat{\boldsymbol{h}}_h$, where $\dot{f}$ is the orbit true anomaly rate. For circular orbits, the true anomaly rate is equal to the mean anomaly rate n.

Finally, the spacecraft body frame B is defined, which is aligned with the spacecraft's principal inertia frame and written as the following:

$$B = \left\{\boldsymbol{r}_{H/N}, \hat{\boldsymbol{b}}_1, \hat{\boldsymbol{b}}_2, \hat{\boldsymbol{b}}_3\right\} \tag{7}$$

The angular velocity vector between the body and inertial frames is given generally as

$${}^{\mathcal{B}}\boldsymbol{\omega}_{B/N} = [\omega_1 \quad \omega_2 \quad \omega_3]^T \tag{8}$$

B. Nonlinear Dynamics

With the system reference frames established, the dynamics that underlie this work are next defined. A spacecraft experiencing spherical two-body gravity and other perturbation accelerations obeys the following equations of motion [15]:

$$\ddot{\boldsymbol{r}} = -\frac{\mu}{r^3}\boldsymbol{r} + \boldsymbol{a}_p \tag{9}$$

where $\boldsymbol{r}$ is the inertial spacecraft position vector, μ is the planet's gravitational parameter, and $\boldsymbol{a}_p$ is the inertial perturbing acceleration vector. It is assumed that drag is the sole perturbation force and follows a quadratic model [15]:

$$\boldsymbol{a}_p = \boldsymbol{a}_D = -\frac{1}{2}\beta P(\boldsymbol{v}^T\boldsymbol{v})\hat{\boldsymbol{v}} \tag{10}$$

in which β represents the spacecraft ballistic coefficient, P is used to represent the local atmospheric density, $\boldsymbol{v}$ is the flow-relative velocity of the spacecraft, and $\hat{\boldsymbol{v}}$ is the unit direction of the flow-relative velocity.

Attitude dependence enters into the system primarily through the ballistic coefficient β_d, which depends on the spacecraft's flow-wise projected area A_i. Considering a spacecraft consisting of several flat faceted panels with individual areas A_i, individual drag coefficients $C_{D,i}$, and individual orientations in the body frame $\hat{n}_i$, the spacecraft ballistic coefficient due to a collection of n flow-exposed panels is written using a modified form of the expressions derived by Sutton [10]:

$$\beta = \frac{\sum_{i=1}^{n} C_{D,i}A_i({}^{\mathcal{B}}\hat{\boldsymbol{n}}_i \cdot [BN]^{\mathcal{N}}\hat{\boldsymbol{v}})}{m} \tag{11}$$

The term $A_i({}^{\mathcal{B}}\hat{\boldsymbol{n}}_i \cdot [BN]^{\mathcal{N}}\hat{\boldsymbol{v}})$ will be referred to as the projected area A_p. The drag coefficient $C_{D,i}$ is a complex variable arising from interactions between rarefied atmosphere and a facet's material properties. Some analytical models of gas–surface interactions do include attitude dependence, such as those described by Bird [16] and used in a space context by Sutton [10]. Calculating the impacts of these effects requires detailed knowledge of both the spacecraft's material properties, which vary on orbit due to space weathering effects, and the specific temperature and composition of the local atmosphere. These parameters are difficult to determine in practice. For the purposes of this analysis, it is assumed that surface drag coefficients remain constant over the analysis time period.

C. Nonlinear Relative Dynamics

For spacecraft in LEO, drag forces alone can be used to achieve limited translational controllability. In general, they can only be used to reach orbits with equal inclinations (as drag acts primarily in the orbit plane) and lower energies. Instead of considering the case of general LEO orbital transfer, this Note's scope is restricted to consider only the relative motion between spacecraft experiencing atmospheric drag forces.

Classic relative motion equations describe the motion of a "deputy" spacecraft as seen by a "chief" spacecraft. The positions of these two spacecraft are related by the following expression:

$$\boldsymbol{r}_d = \boldsymbol{r}_c + \boldsymbol{\rho} \tag{12}$$

in which $\boldsymbol{\rho}$ is introduced to represent the relative position between the chief and deputy. Taking two inertial derivatives results in the following relationship between the accelerations:

$$\ddot{\boldsymbol{r}}_d = \ddot{\boldsymbol{r}}_c + \ddot{\boldsymbol{\rho}} \tag{13}$$

From this, the relative acceleration vector is solved for in terms of the chief and deputy accelerations given by Eq. (9):

$$\ddot{\boldsymbol{\rho}} = \ddot{\boldsymbol{r}}_d - \ddot{\boldsymbol{r}}_c \tag{14}$$

$$\ddot{\boldsymbol{\rho}} = -\frac{\mu}{r_d^3}\boldsymbol{r}_d + \boldsymbol{a}_{D,d} + \frac{\mu}{r_c^3}\boldsymbol{r}_c - \boldsymbol{a}_{D,c} \tag{15}$$

in which $\boldsymbol{a}_{D,c}$ and $\boldsymbol{a}_{D,d}$ are used to represent the drag accelerations of the chief and deputy, respectively. Substituting in Eq. (12) results in

$$\ddot{\boldsymbol{\rho}} = -\frac{\mu}{(r_c+\rho)^3}(\boldsymbol{r}_c + \boldsymbol{\rho}) + \frac{\mu}{r_c^3}\boldsymbol{r}_c + \boldsymbol{a}_{D,d} - \boldsymbol{a}_{D,c} \tag{16}$$

D. Linear Relative Dynamics with Drag

The nonlinear dynamics expressed in Eq. (16) provide little a priori analytical insight into the behavior of relative spacecraft motion under drag. To this end, Silva [17] provided one set of analytical expressions for relative motion under the assumption of atmospheric drag, small relative positions and velocities, and circular chief orbits, effectively constituting a "Hill–Clohessy–Wiltshire plus drag" formulation for differential-drag motion. Rotated into the aforementioned Hill frame and taking $\boldsymbol{\rho} = [\,x \quad y \quad z\,]^T$, these equations are

$$\ddot{x} = 2\dot{y}n + 3n^2x - \frac{1}{2}\beta_d P_d n r_c \dot{x} \tag{17a}$$

$$\ddot{y} = -2\dot{x}n - n^2 r_c^2 \frac{1}{2}(\beta_c P_c - \beta_d P_d) - \beta_d P_d n r_c \dot{y} \tag{17b}$$

$$\ddot{z} = -zn^2 - \frac{1}{2}(\beta_d P_d r_c n)\dot{z} \tag{17c}$$

This model neglects the linearized effect of relative altitude variation on the atmospheric density. For an exponential atmosphere, the linearized deputy density would be

$$P_d = P_c e^{-x/H} \approx P_c(1 - x/H) \tag{18}$$

which is accurate within one atmospheric scale height of the chief's position, or approximately 8 km in LEO. However, introducing this linearization to Eqs. (17a–17c) creates a dependence on the atmospheric scale height, which may be only coarsely known. Instead, the variable P_d will be retained.

For static relative equilibria to exist, both the first- and second-order derivatives must be zero. Setting the second-order derivatives equal to zero yields the following expressions:

$$\tfrac{1}{2}\beta_d P_d r_c \dot{x} = 2\dot{y} + 3nx \tag{19a}$$

$$n^2 r_c^2 \tfrac{1}{2}(\beta_c P_c - \beta_d P_d) + \beta_d P_d n r_c \dot{y} = -2\dot{x}n \tag{19b}$$

$$\tfrac{1}{2}(\beta_d P_d r_c n)\dot{z} = -zn^2 \tag{19c}$$

A secular drift term exists in the y direction due to the differential-drag force acting between the deputy and chief, without a dependence on the relative state components. At the same time, we see that conditions exist that permit stable modes in the x and y velocities for nonzero values of x. Additionally, zeroing the first-order derivatives yields

$$0 = 3nx \tag{20a}$$

$$0 = n^2 r_c^2 \tfrac{1}{2}(\beta_c P_c - \beta_d P_d) \tag{20b}$$

$$0 = -zn^2 \tag{20c}$$

which suggests that the system origin is a static equilibrium when the differential-drag term $n^2 r_c^2 (1/2)(\beta_c P_c - \beta_d P_d)$ is zeroed.

As such, in addition to the classic Hill–Clohessy–Wiltshire (HCW) conditions for static equilibria, it is necessary to ensure that the deputy and chief values of the ballistic coefficient and local neutral density match. This condition could be achieved by either using spacecraft with identical geometries and masses (i.e., formation constitution/maintenance) or by selecting different reference attitudes in which both spacecraft display identical ballistic coefficients. For the purposes of this work, the former assumption will be made for the remainder of the presented analysis.

E. Attitude Sensitivity

The linear approximations for both formation dynamics under drag and the effect of attitude on drag forces lend themselves to the application of linear controllability tools. To use these tools, it is necessary to restate the system dynamics in a linear form such that the system behavior is described by

$$\dot{\boldsymbol{x}} = [A]\boldsymbol{x} + [B]\boldsymbol{u} \tag{21}$$

where $[A]$ represents the linearized state dynamics, and $[B]$ represents the linearized control effects matrix.

The second-order relative equations of motion given in Eqs. (17a–17c) contain secular drift terms proportional to the deputy–chief differential drag $(\beta_c P_c - \beta_d P_D)$. Under the assumption of similar deputy and chief geometries, this term goes to zero because $\beta_c = \beta_d$ for identical reference geometries and attitudes and $P_D = P_c$ as $\boldsymbol{\rho}$ goes to $\mathbf{0}$. This assumption is reasonable for station keeping within a formation of identical spacecraft, for which local variations in density are likely small and spacecraft are likely to have similar geometries. Applying this assumption yields the following state dynamics matrix:

$$[A] = \begin{bmatrix} 0 & 0 & 0 & 1 & 0 & 0 \\ 0 & 0 & 0 & 0 & 1 & 0 \\ 0 & 0 & 0 & 0 & 0 & 1 \\ 3n^2 & 0 & 0 & -\frac{1}{2}\beta_d P_d n r_c & 2n & 0 \\ 0 & 0 & 0 & -2n & -\beta_d P_d n r_c & 0 \\ 0 & 0 & -n^2 & 0 & 0 & -\frac{1}{2}(\beta_d P_d r_c n) \end{bmatrix},$$

$$\boldsymbol{x} = \begin{bmatrix} \boldsymbol{\rho} \\ \dot{\boldsymbol{\rho}} \end{bmatrix} \tag{22}$$

Denoting the sensitivity of the deputy ballistic coefficient on attitude as $(\partial\beta_d/\partial\boldsymbol{\sigma}_p)$, where $\boldsymbol{\sigma}_p$ is an arbitrary attitude variation, the sensitivities of the system dynamics to variation in attitude are described by

$$\frac{\partial \ddot{x}}{\partial \boldsymbol{\sigma}_p} = -\tfrac{1}{2} P_d n r_c \dot{x}_0 \frac{\partial \beta_d}{\partial \boldsymbol{\sigma}_p} \tag{23a}$$

$$\frac{\partial \ddot{y}}{\partial \boldsymbol{\sigma}_p} = \left(\frac{1}{2} n^2 r_c^2 P_d - P_d n r_c \dot{y}_0\right)\frac{\partial \beta_d}{\partial \boldsymbol{\sigma}_p} \tag{23b}$$

$$\frac{\partial \ddot{z}}{\partial \boldsymbol{\sigma}_p} = -\frac{1}{2}(P_d r_c n)\dot{z}_0 \frac{\partial \beta_d}{\partial \boldsymbol{\sigma}_p} \tag{23c}$$

A consequence of this linearization is that the relative acceleration partials are dependent upon the selection of initial or selected reference relative velocities. For the purposes of this work, $[B]$ will be evaluated at the desired equilibrium state where $\boldsymbol{\rho} = \mathbf{0}$ and $\dot{\boldsymbol{\rho}} = \mathbf{0}$. By taking the variation from reference attitude $\boldsymbol{\sigma}_p$ as the control input to the system, the B matrix is stated as

$$[B] = \begin{bmatrix} \mathbf{0}_{3\times3} \\ \mathbf{0}_{1\times3} \\ \frac{1}{2}n^2 r_c^2 P_d \frac{\partial \beta_d}{\partial \boldsymbol{\sigma}_p} \\ \mathbf{0}_{1\times3} \end{bmatrix}, \qquad \boldsymbol{u} = \begin{bmatrix} \sigma_{p,1} \\ \sigma_{p,2} \\ \sigma_{p,3} \end{bmatrix} \tag{24}$$

For demonstrative purposes, the specific case of attitude-independent drag coefficients is considered. Attitude-independent drag coefficient models are commonly used throughout the formation flight literature. Under this assumption, all variation in the ballistic coefficient is due to attitude effects on the spacecraft's projected area. To examine these effects, an additional "target" frame T is defined with a corresponding attitude matrix $[TB]$, allowing the expression of the projected attitude as

$$A_p = A_i(\hat{\boldsymbol{n}}^T[TB(\boldsymbol{\sigma}_p)][BN(\boldsymbol{\sigma}_r)]^{\mathcal{N}}\hat{\boldsymbol{v}}) \tag{25}$$

Modified Rodriguez parameters (MRPs) are selected as the attitude parametrization for this linearization to improve the domain of linearity [1]. Without loss of generality, the inertial velocity direction is also rotated into the chief Hill reference frame. Under the assumption of circular orbits, the inertial direction of the velocity vector in the chief reference frame is simply the $\hat{\boldsymbol{h}}_\theta$ unit vector. The per-facet projected area is therefore

$$A_p = A_i(\hat{\boldsymbol{n}}_i^T[TB(\boldsymbol{\sigma}_p)][BH(\boldsymbol{\sigma}_r)]^{\mathcal{H}}\hat{\boldsymbol{v}}) \tag{26}$$

if that σ_p is small such that second-order terms can be neglected [Eq. (29)]:

$$A_p = A_i(\hat{\boldsymbol{n}}_i^T[BN(\boldsymbol{\sigma}_r)]\hat{\boldsymbol{v}} - 4\hat{\boldsymbol{n}}_i^T[\boldsymbol{\sigma}_p\times][BN(\boldsymbol{\sigma}_r)]\hat{\boldsymbol{v}}) \tag{27}$$

This expression contains two primary components: a constant term driven by the selected reference MRP, and a linearized rotational component based on the perturbing MRP. Treating this perturbing MRP as the control input to the system, it is apparent that the partials of the ballistic coefficient are dependent only on this small-angle rotational component:

$$\frac{\partial \beta_d}{\partial \boldsymbol{\sigma}_p} = \frac{1}{m_i}\sum_{i=1}^{n} -4C_{D,i}A_i\hat{\boldsymbol{n}}_i^T \frac{\partial}{\partial \sigma_p}([\boldsymbol{\sigma}_p\times][BN(\boldsymbol{\sigma}_r)]\hat{\boldsymbol{v}}) \tag{28}$$

Here, the properties of the cross product matrix are exploited to simplify the linearization. For arbitrary vectors $\boldsymbol{a}$ and $\boldsymbol{b}$ and for an arbitrary matrix $[Z]$, the following properties hold:

$$[\boldsymbol{a}\times]\boldsymbol{b} = -[\boldsymbol{b}\times]\boldsymbol{a} \tag{29}$$

$$\frac{\partial}{\partial \boldsymbol{x}}[Z]\boldsymbol{x} = [Z] \tag{30}$$

To simplify the notation, the intermediate vector $\hat{\boldsymbol{q}} = [BN(\boldsymbol{\sigma}_r)]\hat{\boldsymbol{v}}$ is introduced. Applying these properties to the derivatives in Eq. (32) yields

$$\frac{\partial \beta_d}{\partial \boldsymbol{\sigma}_p} = \frac{1}{m}\sum_{i=1}^{n} 4C_{D,i}A_i\hat{\boldsymbol{n}}_i^T[\hat{\boldsymbol{q}}\times] \tag{31}$$

which is entirely defined by the spacecraft mass, geometry, and reference attitude.

III. Controllability Analysis and Controller Implementation

A. Controllability Analysis

Equations (17a–17c) and (23a–23c) define a linear set of equations of motion for a deputy–chief pair with the deputy attitude as an input. Although these equations of motion are general with regard to the deputy and chief geometry, a restricted case dealing with identical deputy–chief geometries is used to demonstrate the controllability properties of this system. This can be considered to represent multiple use cases. One example is maneuvering to a predefined reference orbit and attitude during formation constitution (i.e., matching position and velocity with a fictitious chief). For rendezvous with a fictitious chief, it is desirable for the fictional chief orbit to have identical drag parameters to the real deputy. In any of these cases, the system aim is to drive both the relative position and relative velocity states to zero.

The linearized equations derived in Sec. II.E enable the use of straightforward linear analysis tools to demonstrate controllability. A classic approach to controllability for linear systems uses the controllability matrix $[O]$, which is formed as [18]

$$[O] = \begin{bmatrix} [B] & [A][B] & [A]^2[B] & \dots & [A]^{n-1}[B] \end{bmatrix} \tag{32}$$

where n is the dimension of the state space. The column and null spaces of $[O]$ form bases for the controllable and uncontrollable subspaces for the system, respectively. Examining Eqs. (17a–17c) shows that in-plane dynamics are coupled, but the out-of-plane z dynamics are independent. This suggests that the control effects matrix defined by Eq. (24) will allow for the control of both the x and y states and their derivatives.

Due to the symbolic complexity of these expressions, several numerical examples are provided to demonstrate the controllability properties of the linearized system. A reference system consisting of a single flat plate with the dimensions, drag coefficient, and mass based upon those of a 3U CubeSat with a 3 by 3 m drag sail were used to numerically evaluate $[A]$ and $[B]$ for the purposes of forming $[O]$. The specific values used for these properties are listed in Table 1. Orbital elements for both the chief and deputy are given in Table 2. The matrix rank and QR factorization were computed using the NumPy linalg library [19].

Three cases are examined: one in which the reference attitude is zero, representing a facet face on into the flow; one in which the reference attitude is 90 deg, representing a facet edge on into the flow; and one in which the reference attitude is equivalent to a 45 deg rotation about the HCW $\hat{\boldsymbol{h}}_h$ axis, representing an intermediate drag configuration. These configurations are visualized in Fig. 2. The rank of $[O]$ for each configuration, along with the controllable eigenvectors, are listed in Table 3.

This analysis reveals multiple phenomena relating to the system's controllability. First, the selected reference attitude can restore or prevent controllability. This is sensible when considering the nature of the small-attitude assumption as it relates to the area projection term. This dependence is more explicit when considering the area projection in terms of a single principle attitude angle θ; in which case, the projection can be rewritten as

$$\hat{\boldsymbol{n}}^T\hat{\boldsymbol{v}} = \cos(\theta) \tag{33}$$

Table 1 Spacecraft geometric parameters used for numerical controllability analysis

Parameter	Chief value
P_i	2.7346×10^{-14} kg/m^3
A_i	9 m^2
m_i	6 kg
$\hat{\boldsymbol{n}}_i$	$[0 \quad 1 \quad 0]^T$
$C_{d,i}$	2.2

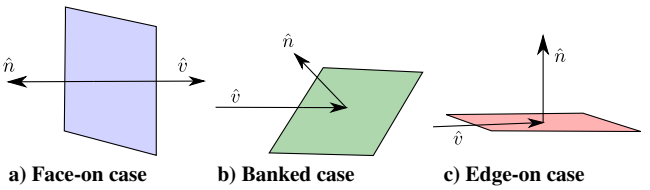

a) Face-on case **b) Banked case** **c) Edge-on case**

Fig. 2 Visualization of face-on, intermediate, and edge-on attitude configurations for a single facet.

Table 2 Orbital elements for both the deputy and chief spacecraft

Orbital element	Chief value	Deputy value
a	230 km+r_{eq}	230 km+r_{eq}
i, deg	45	45.01
e	0	0
Ω, deg	20.0	20.0
ω, deg	30.0	30.0
M_0, deg	20.0	19.99

Evaluating the cosine term about a reference angle θ_r and considering a small perturbation angle θ_p yields

$$\hat{\boldsymbol{n}}^T\hat{\boldsymbol{v}} = \cos(\theta_r + \theta_p) \tag{34}$$

If $\theta_r = 0$, corresponding to the face-on case, the effect of the perturbation angle drops out, explaining the loss of linear controllability. However, the edge-on case also presents an issue. For a physical plate, rotation in either direction represents an increase in the projected area. If the chief is assumed to be uncooperative, this means that the effective control input can never produce a negative acceleration and, as such, a linear model cannot effectively approximate its behavior. It is only in the banked case that control authority is provided about the described equilibrium condition in which the deputy and chief ballistic coefficients are equal. This is illustrated in Fig. 3, which demonstrates the variation of a single-plate deputy drag coefficient with attitude for reference attitude configurations facing into the flow, banked into the flow, and edge on into the flow, respectively. From this figure, it is apparent that the controllability of the system for $\theta_r = 90$ deg is an artifact of the manner in which the system is linearized, due to the discontinuity at the facet edge.

This analysis provides a framework to understand admissible conditions and geometries for differential-drag control inside and outside the linear regime. Differential-drag formation flight requires that the deputy–chief pair be able to achieve both positive and negative relative accelerations from drag. In the attitude-only noncooperative rendezvous case considered here, this requires that the deputy geometry and attitude allow it to both increase and decrease its drag profile relative to the chief.

Using the intermediate case angle as the reference angle, this analysis reveals that the in-plane states and velocities are controllable from attitude-driven drag alone. This is consistent with both the well-known in-plane coupling expressed by the Hill–Clohessy–Wiltshire equations for linear relative motion and the planar nature of drag forces on spacecraft. Additionally, these results agree with results found in the literature for this class of control [3]. In comparison to differential-drag studies that use differential mean orbit elements (such as Ref. [20]) and show that relative mean elements corresponding to components of in-plane motion are uncontrollable, these results can be considered as using short-period behavior (which is lost in the averaging analysis) to gain controllability in plane at the expense of requiring small separation distances and maneuver time periods to remain in the linear regime.

Table 3 Controllability analysis results

Bank angle, deg	Rank ($[O]$)	Stabilizable state-space eigenvectors
0	0	— —
45	4	$[\hat{x}\ \ \hat{y}\ \ \hat{\dot{x}}\ \ \hat{\dot{y}}]$
90	4	$[\hat{x}\ \ \hat{y}\ \ \hat{\dot{x}}\ \ \hat{\dot{y}}]$

B. Linear Control Performance

1. *Single-Facet Control*

Per the previous section, a subspace of the linearized system has been demonstrated to be linearly controllable. To this end, a straightforward linear control law based on linear quadratic regulator (LQR) was developed and implemented for the sample linear system based on Table 1. Results are provided for two selected control objective weights: one that emphasized the fast-state performance ("fast case"), and one that emphasized economical use of the control input (the "economic case"). Both the state gains $[Q]$ and the control gains $[R]$ are selected to be diagonal, with elements of the magnitude stated in Table 4. The latter can be analogously considered as minimizing the variance from the desired reference attitude. For demonstration purposes, the control objective is to drive the deputy spacecraft to the chief position and velocity.

With respect to the linearized system, both controls are found to be stabilizing, resulting in the state trajectories found in Figs. 4 and 5. The commanded attitude MRPs are displayed in Fig. 6. Notably, the commanded attitudes in the fast-state case vary far outside the domain in which MRP switching would typically be used ($\sigma^2 = 1$), suggesting that the system violates the small angle assumption critical to the linearization. Additionally, it is noted that the fast-state case displays substantial oscillation even after notionally reaching the reference states, although it is apparent from Fig. 4a that its behavior is convergent toward the origin. The Hill–Clohessy–Wiltshire dynamics are well known to exhibit oscillatory modes in the form of a two-by-one ellipse in the planar states; as a result of the small control authority afforded by drag, it is difficult to completely eliminate this behavior.

To provide further validation of this approach, the linear controller was implemented on a system following the full nonlinear equations of motion found in Eq. (15) under the same initial conditions and parameters used to generate the linearized system (i.e., those found in Tables 1–4). The selected scenario represents a slot-hopping maneuver, in which a spacecraft maneuvers to a selected reference location and attitude ahead of its current position on orbit. A small inclination difference is included to demonstrate the control's lack of influence on out-of-plane motion, as expected. The results of these simulations under both control strategies can be found in Figs. 7 and 8. Attitude trajectories for these cases are shown in Fig. 9.

Notably, the LQR controller derived for the linear system provides similar performance for the nonlinear system using the economic case's control gains. This both validates the linearizations used to derive the LQR controller and demonstrates the applicability of the linearized system to the "real" problem at hand. However, the results of the fast case, which display state divergence from the reference,

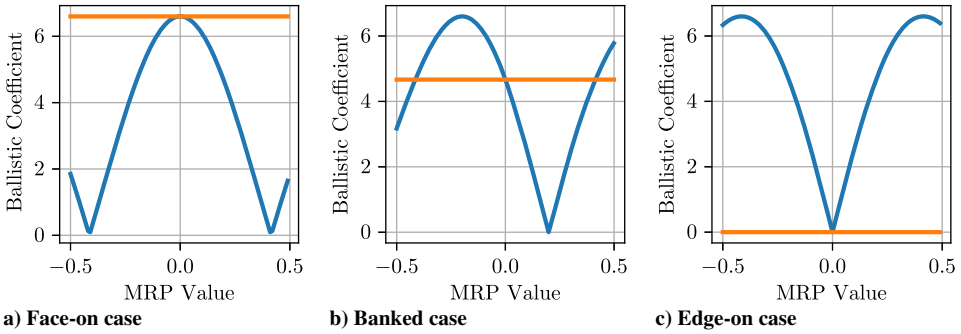

a) Face-on case b) Banked case c) Edge-on case

Fig. 3 Deputy (blue) and chief (orange) ballistic coefficients using reference numbers from Table 1. Results shown for face-on, banked, and edge-on reference attitudes.

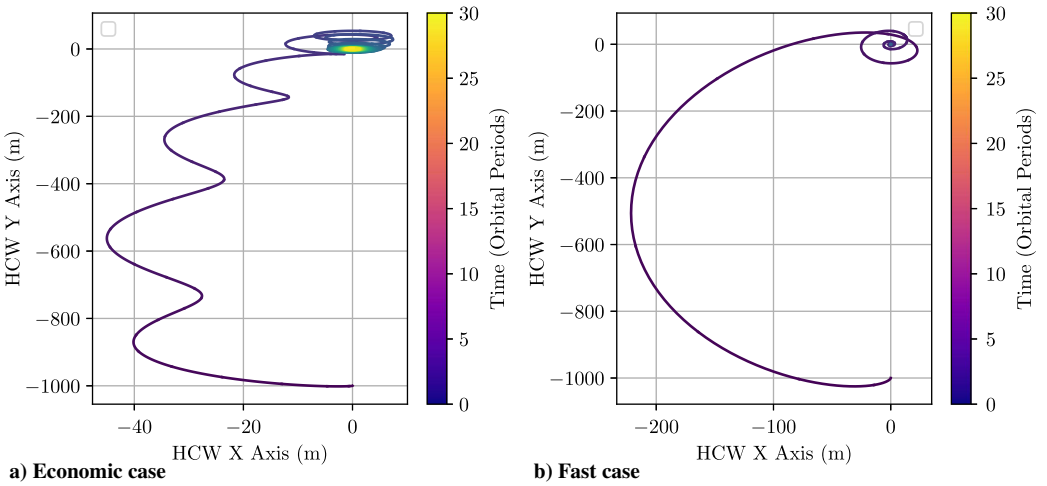

Fig. 4 HCW *x*- and *y*-state evolutions under linear dynamics with LQR-derived controller.

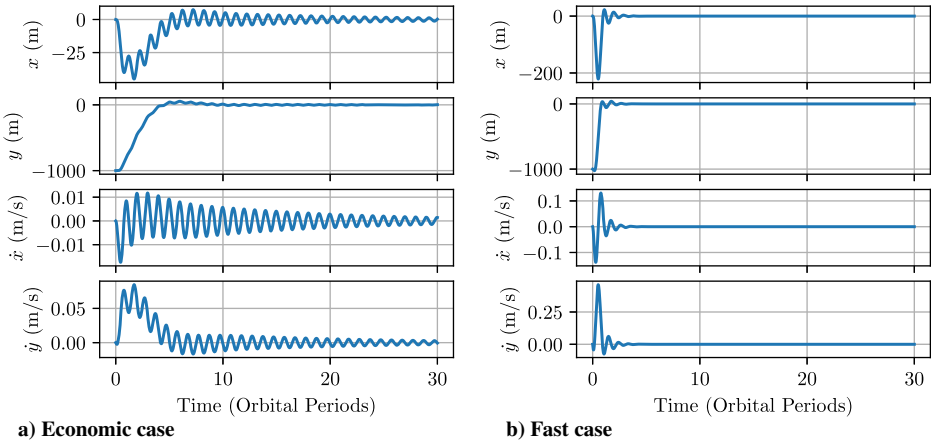

Fig. 5 Deputy relative position and velocity state trajectories in the chief Hill frame under attitude-driven control simulated on the linear system.

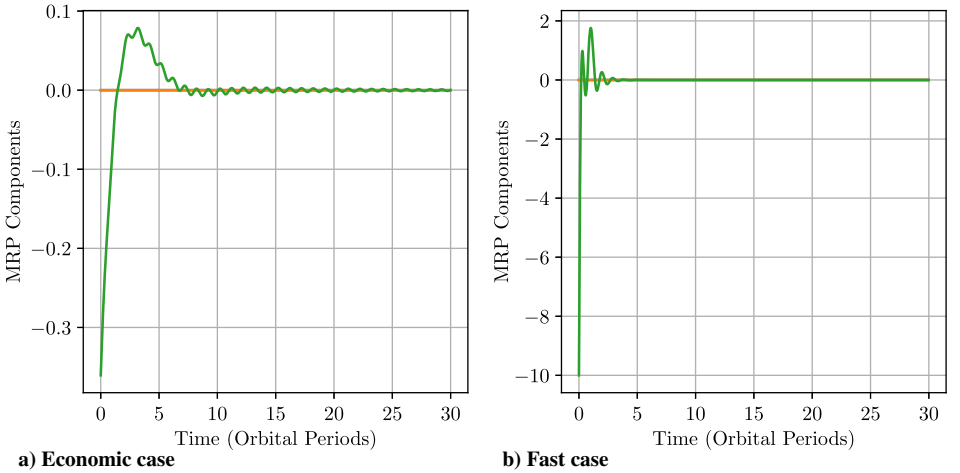

Fig. 6 Flow-relative attitude MRP component generated by LQR-derived controller using linear dynamics under different control weights: perturbed MRP value (green), and reference value (orange).

demonstrate limitations of the linearization approach. In the fast case, the relatively large elements of $[B]$ cause the controller to request large attitudes outside of the linear regime, which is a behavior shown in the linear system through Fig. 6b.

These results demonstrate the need for large penalties for control use in the linearized attitude-driven case. Nonlinearities present in the assumed input (the spacecraft's attitude) are the dominant drivers of nonconvergence for the controlled system. These results were used as guidelines for the development of additional simulations to address other aspects of the system.

2. *Multifaceted Performance*

An expected benefit of this approach is the ability to add additional facets to the dynamic model to further approximate the geometry of a spacecraft. To demonstrate this advantage, the slot-hopping scenario described in Table 2 was repeated with a cuboid spacecraft representing a 3U CubeSat flying obliquely into the flow. The resulting attitude and Hill-frame trajectory are shown in Fig. 10. The more complex, three-dimensional geometry represented by the collection of facets results in additional nonzero terms along the row corresponding to $\dot{y}$ in the control matrix $[B]$; as such, the controller

Table 4 Selected control gains for economic and fast cases

Control design variable	Economic case values	Fast case values
Q	0.1	1
R	1e7	1e4
dt	5s	5s

makes additional use of the corresponding component of the attitude MRP, resulting in a similar overall control magnitude but smaller axiswise components to the single-panel case.

3. Ballistic-Coefficient Variation

Large differences in maximum and minimum ballistic coefficients can produce large relative accelerations, and therefore provide better relative motion control performance than small ones. To this end, the relative controllability of the scenario presented in Sec. III.B.1 is studied under varied plate areas (of which ballistic coefficients are a linear function) with all other factors held constant.

Figure 11 shows the attitude and in-plane trajectories for the nominal-, high-, and low-area cases (Table 5). These results show that control convergence is maintained even with order-of-magnitude differences in the ballistic coefficient. As expected, spacecraft with smaller facet areas require more time to converge than spacecraft with larger facets, reflecting the impact of area on the ballistic coefficient. Notably, the control uses larger deviations from the reference state for control when a larger panel area is available; this is a result of the in-plane coupling predicted by the linearized dynamics because larger y-direction velocities would necessarily produce larger x-direction velocities, and therefore deviations.

C. Performance Under Mismodeled Dynamics

1. Impact of Mismodeled Atmosphere

Even about the Earth, neutral atmospheric density is notoriously difficult to predict. The structure of this approach to linear control necessitates the prediction of atmospheric density to formulate the

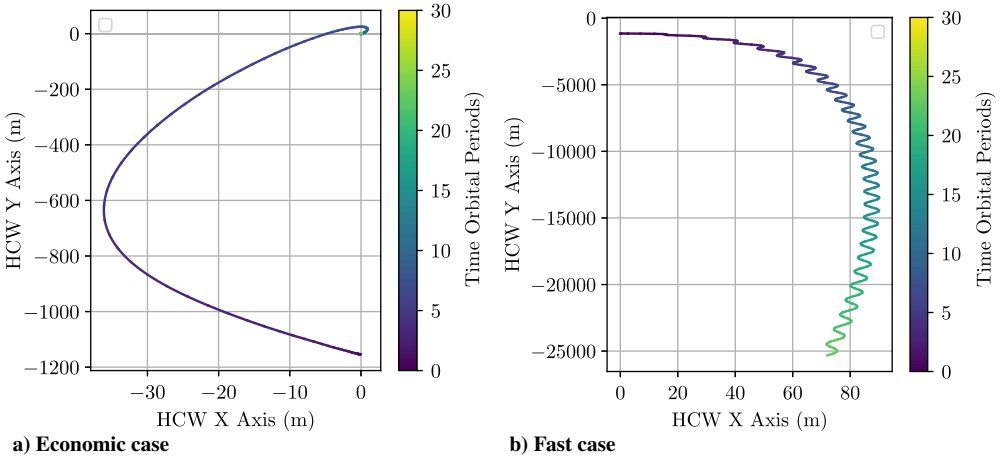

a) Economic case **b) Fast case**

Fig. 7 HCW x- and y-state evolutions under the LQR-derived controller on the assumed nonlinear system.

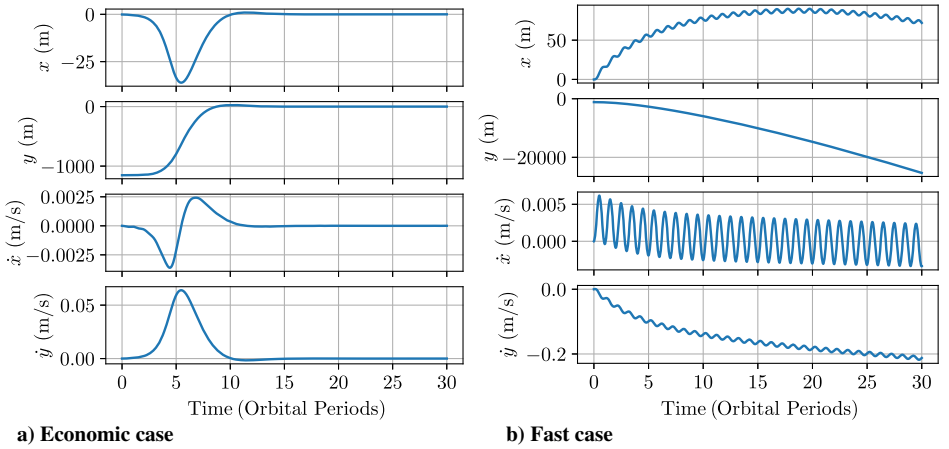

a) Economic case **b) Fast case**

Fig. 8 Deputy relative position and velocity state trajectories in the chief Hill frame under attitude-driven control.

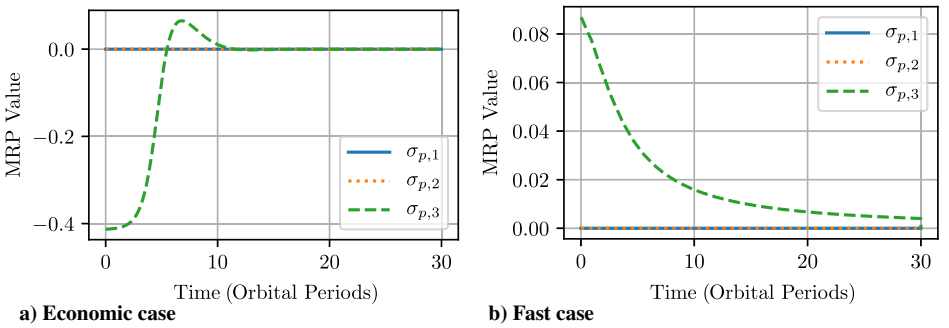

a) Economic case **b) Fast case**

Fig. 9 Flow-relative attitude MRP component generated by the LQR-derived controller. Requested MRPs are transformed to the unit set.

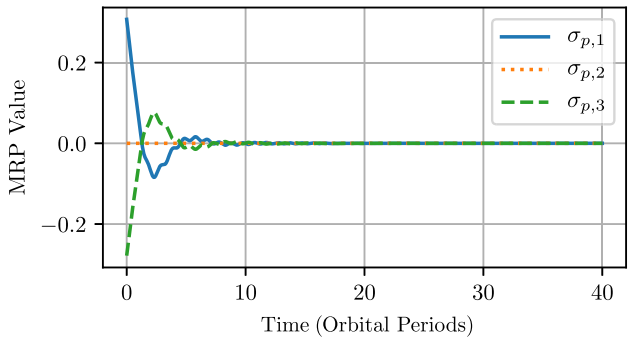

a) Commanded MRP trajectories

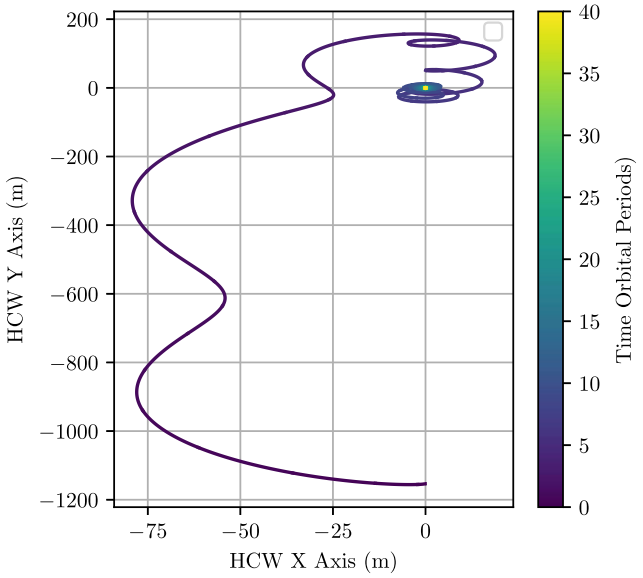

b) In-plane trajectories in the hill frame

Fig. 10 Control performance for a CubeSat represented by three facets.

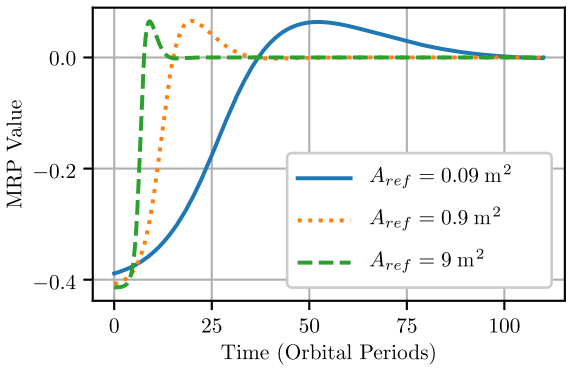

a) Commanded MRP trajectories

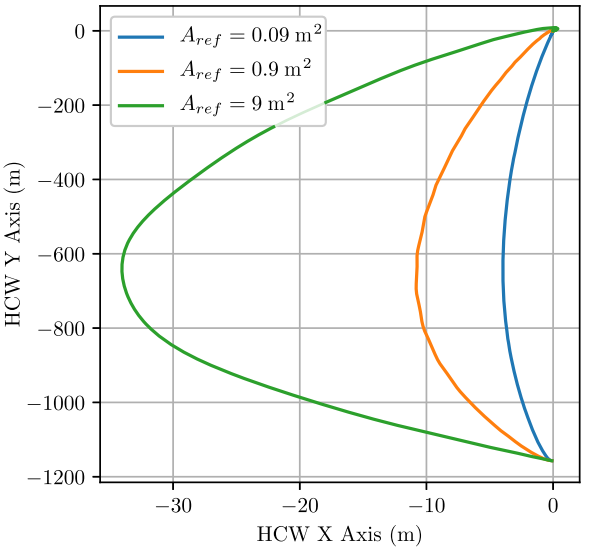

b) In-plane trajectories in the hill frame

Fig. 11 Control performance for various areas and resulting β values.

linearized models that depend on estimates of a base atmospheric density. To identify the effect of mismodeled atmospheric density on the controller's effectiveness, the same scenario used in Sec. III.A was run with the real density offset from the density used to construct the controller by 40% ($0.6\rho_0$ and $1.4\rho_0$, respectively).

Although the model dynamics are linearly dependent on the exponentially varying atmosphere, a degree of robustness is maintained by the assumption that the relative spacecraft-reference dynamics occur for nearby orbits (∼10 km). Under the assumed exponential atmospheric model, this distance falls within one atmospheric scale height of the reference orbit, which is beneath the point at which higher-order terms in the series expansion of an exponential atmospheric model become substantial. As shown in Fig. 12, variation in the atmospheric density from the design value simply changes the rate of convergence of the controller, resulting in under or overshoot.

2. *Convergence with Unmodeled J_2*

The accelerations from $J2$ are, alongside atmospheric drag, the dominant perturbations for spacecraft in LEO. Although $J2$ is not included in the dynamical model used to construct the control scheme, the presence of feedback control suggests that the system may still be stable under the presence of unmodeled dynamics such as $J2$. To address this concern, the scenario defined by Table 2 was redone with an increased initial separation (∼10 km of along-track separation) and the addition of unmodeled $J2$ accelerations using the following inertial expression:

$$\mathcal{N}\boldsymbol{a}_{J2} = -\frac{3}{2}J_2\frac{\mu}{r^2}\frac{r_{\text{eq}}^2}{r}\begin{pmatrix}\left(1-5\left(\frac{z}{r}^2\right)\right)\frac{x}{r}\\ \left(1-5\left(\frac{z}{r}^2\right)\right)\frac{y}{r}\\ \left(3-5\left(\frac{z}{r}^2\right)\right)\frac{z}{r}\end{pmatrix} \tag{35}$$

More important, the differential disturbance from J_2 goes to zero as the relative position goes to zero; as such, the inclusion of disturbances from J_2 will not affect the equilibria of the system.

The results of this analysis are shown in Fig. 13, which demonstrates that the resulting controller behavior drives the spacecraft into a neighborhood about the target position. Compared to Fig. 7a, more periodic oscillations are seen. These oscillations are consistent with the comparison of osculating vs mean controllability described in Sec. III.A; the resulting oscillations are partially the result of attempting to control short-period variations caused by J_2.

From the demonstrated scenario, the controller still converges to a stable position near the designated position in the controlled axes in a time comparable to the unperturbed case; however, oscillations that are periodic with the orbit period resulting from $J2$ are clearly present early in the trajectory. Regardless, this suggests that the described attitude-only approach has merit for the control of realistically sized spacecraft in LEO.

Table 5 Low, nominal, and high plate areas used to test the performance impact of ballistic coefficients

Case	Area, m^2
Low area	0.09
Nominal area	0.9
Large area	9

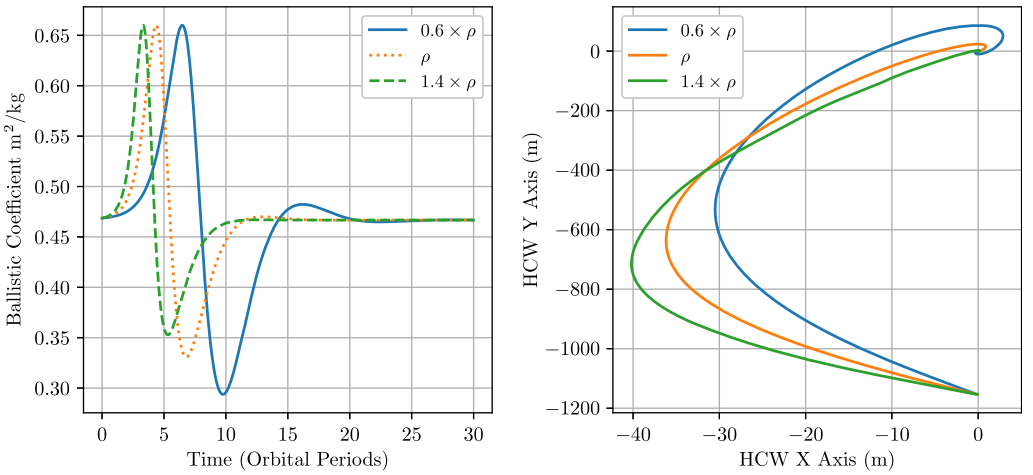

a) Ballistic coefficient variation: the red line represents the "reference" ballistic coefficient

b) In-plane HCW trajectories corresponding to different density cases

Fig. 12 Control performance under mismodeled atmospheric density. Convergence is achieved with both higher and lower variations.

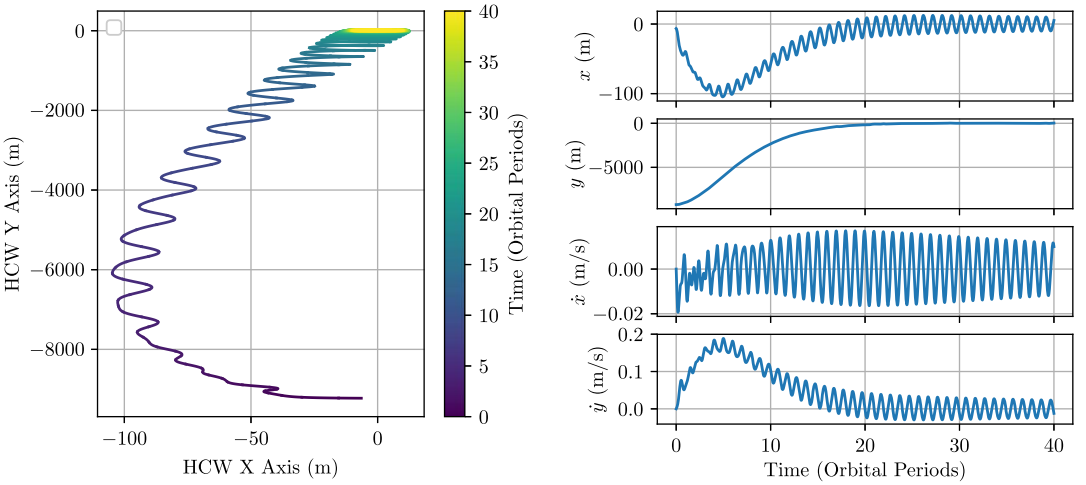

a) In-plane hill frame deputy trajectory

b) Deputy in-plane state trajectories

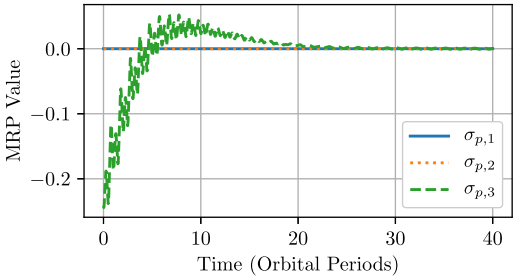

c) Deputy attitude components over time

Fig. 13 Control performance under unmodeled $J2$ dynamics.

IV. Conclusions

A novel framework for the consideration of differential-drag formation flight as a linear formation control problem has been presented and derived. For spacecraft pairs with intermediate drag geometry-attitude configurations, linear controllability is possible from small-attitude motion alone, without the assumption of additional drag surfaces. These results provide an alternative perspective on the controllability and stability of formation flight under the consideration of atmospheric drag. In the described linearization; simulations show that the attitude linearization is a primary constraint for the design of controllers. Despite this, controllers based on this formulation of the differential-drag formation flight problem show convergence in the presence of unmodeled variations in atmosphere and $J2$ accelerations while providing physical insight into the problem structure.

Acknowledgments

This work was supported by the U.S. Department of Defense National Defense Science and Engineering Graduate Fellowship Program, the U.S. Air Force Research Laboratory Space Scholars Program, and the University of Colorado Boulder (CU) Smead Scholars Fellowship.

References

[1] Schaub, H., and Junkins, J. L., *Analytical Mechanics of Space Systems*, 3rd ed., AIAA, Reston, VA, 2014, pp. 209–210. https://doi.org/10.2514/4.102400

[2] Marcos, F., Bowman, B., and Sheehan, R., "Accuracy of Earth's Thermospheric Neutral Density Models," *AIAA/AAS Astrodynamics Specialist Conference and Exhibit*, AIAA Paper 2006-6167, 2006. https://doi.org/10.2514/6.2006-6167

[3] Pérez, D., and Bevilacqua, R., "Differential Drag Spacecraft Rendezvous Using an Adaptive Lyapunov Control Strategy," *Acta Astronautica*, Vol. 83, Feb. 2013, pp. 196–207. https://doi.org/10.1016/j.actaastro.2012.09.005

[4] Kumar, B. S., Ng, A., Yoshihara, K., and De Ruiter, A., "Differential Drag as a Means of Spacecraft Formation Control," *IEEE Transactions on Aerospace and Electronic Systems*, Vol. 47, No. 2, 2011, pp. 1125–1135. https://doi.org/10.1109/TAES.2011.5751247

[5] Gangestad, J. W., Hardy, B. S., and Hinkley, D. A., "Operations, Orbit Determination, and Formation Control of the AeroCube-4 CubeSats," *Proceedings of the AIAA/USU Conference on Small Satellites*, Vol. SSC13, Utah State Univ., Logan, Utah, 2013, Paper SSC13-X-4, https://digitalcommons.usu.edu/smallsat/2013/all2013/116/.

[6] Horsley, M., Nikolaev, S., and Pertica, A., "Small Satellite Rendezvous Using Differential Lift and Drag," *Journal of Guidance, Control, and Dynamics*, Vol. 36, No. 2, 2013, pp. 445–453. https://doi.org/10.2514/1.57327

[7] Foster, C., Hallam, H., and Mason, J., "Orbit Determination and Differential-Drag Control of Planet Labs Cubesat Constellations," *Advances in the Astronautical Sciences*, Vol. 156, 2016, pp. 645–657.

[8] Dell'Elce, L., and Kerschen, G., "Optimal Propellantless Rendez-Vous Using Differential Drag," *Acta Astronautica*, Vol. 109, April–May 2015, pp. 112–123. https://doi.org/10.1016/j.actaastro.2015.01.011

[9] Harris, A. T., Petersen, C., and Schaub, H., "Linear Coupled Attitude-Orbit Control Through Aerodynamic Forces," *AIAA SciTech*, AIAA Paper 2018-0962, 2018. https://doi.org/10.2514/6.2018-0962

[10] Sutton, E. K., "Effects of Solar Disturbances on the Thermosphere Densities and Winds from CHAMP and GRACE Satellite Accelerometer Data," Ph.D. Thesis, Univ. of Colorado, Boulder, Boulder, CO, Oct. 2008.

[11] Pilinski, M., "Dynamic Gas-Surface Interaction Modeling for Satellite Aerodynamic Computations," Ph.D. Thesis, Univ. of Colorado, Boulder, Boulder, CO, 2011, https://scholar.colorado.edu/asen_gradetds/37 [retrieved 2019].

[12] Filipe, N., and Tsiotras, P., "Adaptive Position and Attitude Tracking Controller for Satellite Proximity Operations Using Dual Quaternions," *Advances in the Astronautical Sciences*, Vol. 150, April 2014, pp. 2313–2332. https://doi.org/10.2514/1.G000054

[13] Huo, M., Zhao, J., Xie, S., and Qi, N., "Coupled Attitude-Orbit Dynamics and Control for an Electric Sail in a Heliocentric Transfer Mission," *PLoS ONE*, Vol. 10, No. 5, 2015, Paper e0125901. https://doi.org/10.1371/journal.pone.0125901

[14] Mu, J., Gong, S., and Li, J., "Coupled Control of Reflectivity Modulated Solar Sail for GeoSail Formation Flying," *Journal of Guidance, Control, and Dynamics*, Vol. 38, No. 4, 2015, pp. 740–751. https://doi.org/10.2514/1.G000117

[15] Vallado, D. A., *Fundamentals of Astrodynamics and Applications*, Space Technology Library, 4th ed., Microcosm Press, Hawthorne, CA, 2013, pp. 551–569.

[16] Bird, G. A., *Molecular Gas Dynamics and the Direct Simulation of Gas Flows*, Inelastic Collisions and Surface Interactions, Oxford Univ. Press, New York, 1994, pp. 120–121, Chap. 5.

[17] Silva, E. D., "A Formulation of the Clohessy-Wiltshire Equations to Include Dynamic Atmospheric Drag," *AIAA/AAS Astrodynamics Specialist Conference*, AIAA Paper 2008-6444, 2008. https://doi.org/10.2514/6.2008-6444

[18] Brogan, W. L., *Modern Control Theory*, 3rd ed., Prentice–Hall, Englewood Cliffs, NJ, 1991, pp. 373–386.

[19] Jones, E., Oliphant, T., Peterson, P., et al., "SciPy: Open Source Scientific Tools for Python [online database]," 2017, http://www.scipy.org/ [retrieved 12 Jan. 2017].

[20] Ben-Yaacov, O., and Gurfil, P., "Long-Term Cluster Flight of Multiple Satellites Using Differential Drag," *Journal of Guidance, Control, and Dynamics*, Vol. 36, No. 6, 2013, pp. 1731–1740. https://doi.org/10.2514/1.61496